University of South-Eastern Norway

www.usn.no

FMH606 Master's Thesis 2022

Chemometric analysis of a new benchmark CO_2 capture solvent

Saeed Jahanshahi

Faculty of Technology, Natural sciences and Maritime Sciences
Campus Porsgrunn

University of South-Eastern Norway

www.usn.no

Course: FMH606 Master's Thesis, 2022

Title: Chemometric analysis of a new benchmark CO_2 capture solvent

Number of pages: 34

Keywords: CO_2 capture, partial least square regression, multivariate data analysis, FTIR spectroscopy, CESAR1, corrosion, NMR

Student: Saeed Jahanshahi

Supervisor: Zulkifli Idris, Jayangi Wagaarachchige, Klaus-J. Jens and Maths Halstensen

External partner: Technology Center Mongstad

University of South-Eastern Norway

www.usn.no

Summary:

Greenhouse gases have challenging consequences on climate change and CO_2 is one of the most effective elements in this issue. the methods to mitigate these effects such as capturing the carbon dioxide are the aim of this project. CESAR1 (27 wt% 2-amino-2-methyl-1-propanol+13 wt% Piperazine) as an aqueous solution is the main solution to consider in this project.

Many experiments have been implemented in this study to evaluate this solution. FTIR, pH as well as density measurements are thoroughly studied. All data is evaluated in Unscrambler with the PLS-R method. However, NMR results could not be prepared because of a delayed response from the SINTEF company as well as titration due to several errors. But all experiments that have been completed during this study, were given practical and considerable information about the CESAR1 solution.

pH and density measurements are performed to give results about the effects of loading CO_2 in the CESAR1 solution.

FTIR test is performed to determine the composition of the CESAR1. A series of tests have been done to analyze the effect of CO_2 on CESAR1 solution.

According to the PLS-R analysis, it has been reached to the composition of the CESAR1 solution and how the CO_2 loaded affected the investigations.

From my findings, I can conclude that the FTIR technique is an effective method for the decomposition of this solution to capture carbon dioxide.

Preface

This project aims to investigate the CESAR1 solution to capture carbon dioxide and analysis of optimization of it. I worked with Mongstad company and the University of South-Eastern Norway to improve this solution and detail its characterization and apply this method at a company level.

The project was complete and extensive, and I had interesting results; I did loads of data analysis. Nevertheless, I encountered some issues. The most important one was related to the time limit for my results from the SINTEF company as well as the technical problem of titration device in the university. It was a significant obstacle to do all these experiments for the first time in my career and to take the time then to analyze them. There were limited literature resources on some topics. So, future work is necessary on the subject to further analyze the data and focus on other promising experiments including titration, and NMR tests. I wish to thank my supervisors, Professor Klaus-J. Jens, Associate Professor Maths Halstensen, ph.D. Jayangi Wagaarachchige, and Associate Professor Zulkifli Idris, without their cooperation I would not have been able to conduct this analysis. Finally, I thank the University of South-Eastern Norway and Technology Center Mongstad for providing materials and laboratory rooms.

I hope the reading will interest you,

Porsgrunn
10th of May 2022

Saeed Jahanshahi

Contents

Nomenclature

AMP= 2-amino-2-methyl-1-propanol

CCS= Carbon dioxide capture and storage technique

DEA= diethanolamine

DIPA= di-isopropanolamine

FTIR= Fourier transform infrared spectroscopy

IEA= International Energy Agency

IGCC= Integrated gasification combined cycle

MDEA= N-methyldiethanolamine

MEA= monoethanolamine

NMR= Nuclear magnetic resonance

2-PE= 2-piperidineethanol

PLS-R= Partial least-squares regression model

PZ= Piperazine

RMSE= Root mean square error

SEM= Scanning electron microscopy

TEA= triethanolamine

1 Introduction

One of the most struggling problems during these years is global warming as well as climate change. it is a concern for the earth and the effect of greenhouse gas emissions in particular carbon dioxide is the main reason that makes global warming more complicated. A classification that explains generally the main sources of carbon dioxide generation is illustrated in Figure 1.1 [1]. International Energy Agency (IEA) announced that the total global emissions of CO_2 for coal and crude oil are in the most range in comparison to natural gas. Because of being cheap and the availability of coal, it uses as the most preferred fossil fuel for electricity generation. As a result, coal produces the most carbon dioxide consequently [2]. The emission of CO_2 to the atmosphere affects climate change and a technology namely CO_2 capture can mitigate the negative influence of greenhouse gases considerably. The CO_2 capture and storage (CCS) technique is employed to remove this CO_2 in the process of electricity generation which is divided into three main categories including pre-combustion, post-combustion, and oxy-combustion [2,3]. According to the industry application as well as the most researched techniques in CO_2 capture, these three methods can be ordered as follows: post-combustion > pre-combustion > oxy-fuel combustion [2]. Figure 1.2 demonstrates the combustion processes of carbon dioxide capture [3].

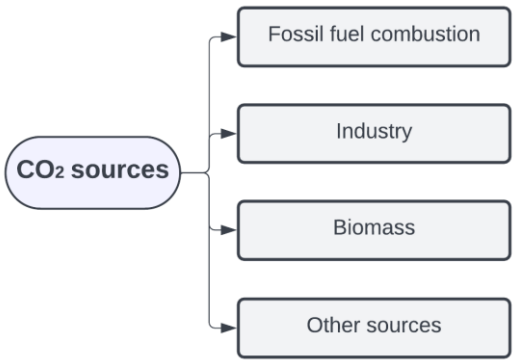

Figure 1.1: Main sources of carbon dioxide [1].

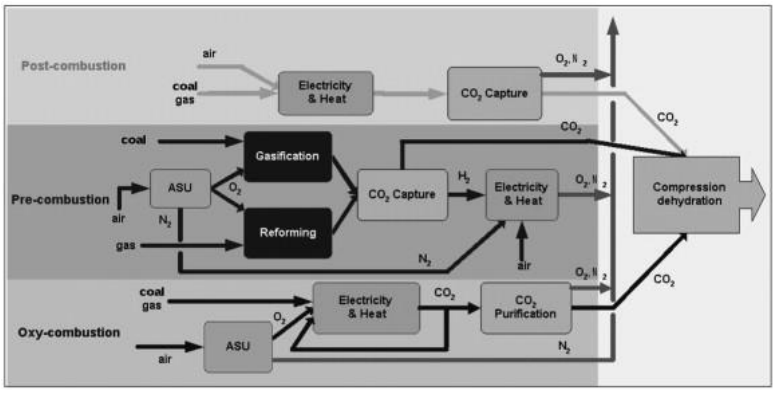

Figure 1.2: The processes of CO_2 capture [3].

CO_2 is well-known as an acid gas and removing it eventuates in both increased heating value of natural gas and less corrosive pipelines [4]. To separate carbon dioxide, the absorption technique is the most applicable method. Figure 1.3 shows the separation techniques for CO_2 [1].

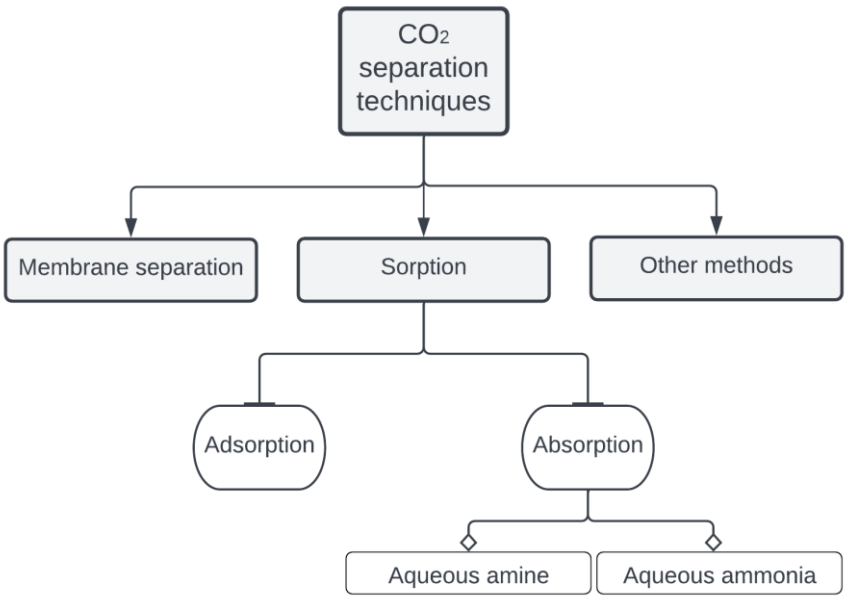

Figure 1.3: Classification of CO_2 separation methods [1].

Alkanolamines as an aqueous solution are employed in this technique. The most noticeable alkanolamines in the industry for the process of carbon dioxide removal are monoethanolamine (MEA), diethanolamine (DEA), N-methyldiethanolamine (MDEA), di-isopropanolamine (DIPA), triethanolamine (TEA), 2-piperidineethanol (2-PE), and 2-amino-2-methyl-1 propanol (AMP) [5,6].

Several properties can define a solvent as an ideal solvent such as low absorption heat, low amine volatility, low cost, low corrosivity, low viscosity, high cyclic capacity, fast reaction kinetics, high thermal degradation, and high resistance to oxidation [7]. Amine solutions have a high range of absorption of CO_2 as well as more efficient in comparison to other solutions [4,8,9] and utilize for gas cleaning inside the flue and react fast with carbon dioxide [10]. Although they have some drawbacks such as being expensive, losing solvent, and requiring energy [5], the combination of 2-amino-2-methyl-1-propanol (AMP) and piperazine (PZ) mitigates high energy requirement and causes to react CO_2 with PZ more with high CO_2 loading capacity [9]. This solvent is called CESAR1 which is included 27 wt% AMP and 13 wt% PZ [11]. It is proved that PZ has a considerable effect on the rate of CO_2 capture and can enhance it even if is a small amount [6].

Adding Piperazine to the AMP solution which has a low reaction rate, increases the rate of CO_2 absorption [6,12] because of the higher reaction rate, oxidation resistance, thermal degradation, and cyclic structure of PZ [8,13,14]. It is approved that in the absorption process the highest ratio of AMP and PZ without solid precipitates at 40 ℃ is 40 wt% amine [8]. During the carbon

dioxide absorption process by AMP and PZ solvent, several components including carbamates, and bicarbonates have been identified [9].

Mangalapally and Hasse studied about CESAR1 and they reported that the regeneration energy was reduced by 20% and the circulation rate of the solvent decreased by 45% in comparison to MEA [15].

Zhang et al. indicated that the regeneration of AMP is faster than other amines categories including less loss of absorption capability. Based on their findings the order for the performance of regeneration is AMP > MDEA > DEA > MEA [5].

The absorption of CO_2 containing less than 15% carbon dioxide concentration was studied at the atmospheric pressure [16–18]. It is limited to implementing the test at high pressure.

Godini et al. conducted the absorption of CO_2 as well as H_2S in different conditions at higher pressure (more than 1.0 MPa) with increasing the ratio of the flow rate (L/G). The consequence showed that the increase in both parameters eventuated in the enhanced efficiency of absorption [19].

Dash et al. evaluated a simulation model of 8 wt% PZ and 22 wt% AMP at more than 2.0 MPa pressure with the same ratio of L/G which is reported for higher carbon dioxide capture result [20].

1.1 CO_2 capture techniques

1.1.1 Post-combustion

Post-combustion is like that once the fuel is being completely burned with air, CO_2 would be captured in the exhaust gases [3]. The produced flue gas by fossil fuel combustion follows the reaction 1.1 [2].

$$C_xH_y + z(O_2 + 3.76N_2) \rightarrow aCO_2 + bH_2O + cO_2 + dN_2 \quad \text{(R1.1)}$$

The stoichiometric coefficients a, b, c, and d as productions hinge upon the coefficients of x, y, and z as reactants.

Although the main products in this reaction are CO_2, H_2O, unreacted O_2, and N_2, other gases such as SO_x, NO_x, and fly ash produces which are impurities in the reaction and consequence of the degradation of amine solvent. These impurities remove before CO_2 capture as Figure 1.4 demonstrates. During the post-combustion process, the CO_2 concentration is 10-15% for coal and 3-8% for natural gas [2].

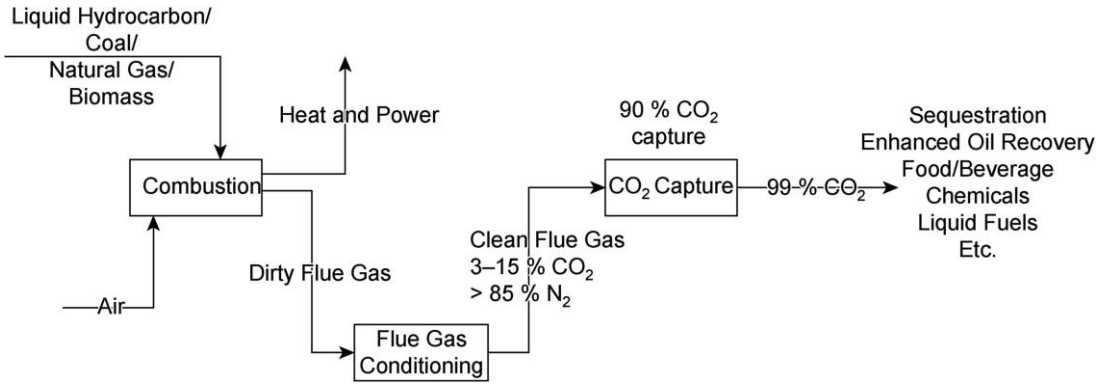

Figure 1.4: CO_2 capture through the post-combustion process [2].

1.1.2 Pre-combustion

In pre-combustion, the process of capturing begins after the formation of CO to CO_2 and before fuel combustion [3]. In other words, the CO_2 captures previously by a technique namely IGCC (integrated gasification combined cycle). Figure 1.5 shows the pre-combustion CO_2 capture. In this technique, the production of syngas is implemented by gasification of fossil fuels with water or steam. The percentage of carbon dioxide in the syngas is different between 5 to 15% and the productions are including both gaseous (H_2, CO_2) and liquid phases (methanol, dimethylether). The produced hydrogen can be utilized for electricity applications such as electric vehicles [2].

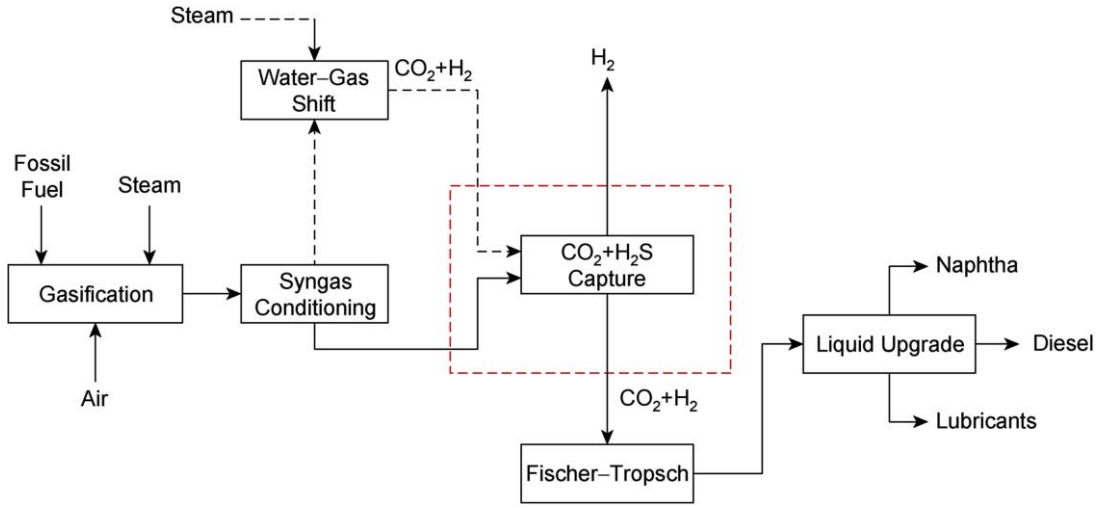

Figure 1.5: CO_2 capture through the pre-combustion process [2].

1.1.3 Oxy-fuel combustion

The process of oxy-combustion is about oxygen combustion with exhaust gas recycling to remove incondensable gasses by CO_2 flow purification [3]. The main object of this method is to enhance the performance of combustion. This is accomplished by using pure oxygen (O_2) rather than air to burn the fuel (Figure 1.6). The CO_2 concentration in this process through the flue gas is 70-90%. This concentration and the combination of water and carbon dioxide in the flue clarify that condensation or liquefaction would be feasible to capture CO_2.

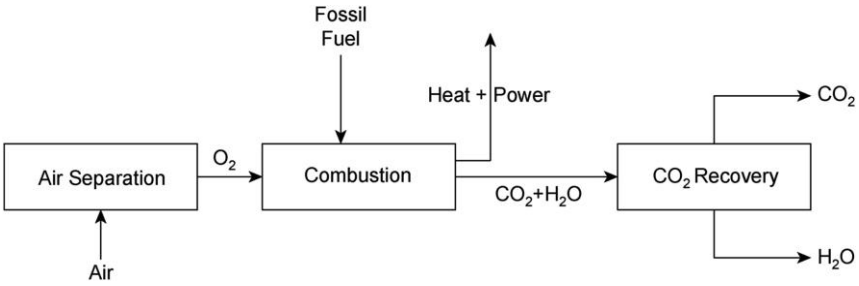

Figure 1.6: CO_2 capture through the oxy-fuel combustion process [2].

1.2 CO_2 capture via amine aqueous solution

The absorption method with an aqueous solution to capture carbon dioxide requires two columns including an absorber as well as a stripper individually. In the absorber column, the gases inside the flue contact with the mixture of amine and water. CO_2 removal will be implemented by a weak bonding between carbon dioxide and amine. Then, these weak bonds transfer to the stripper column. After that, the solvent will heat to release CO_2 to regenerate. This regenerated amine is still utilized for the same process of CO_2 capture again. The procedure occurs through the following chemical reactions [1]:

1. Carbamate formation:

$$CO_2 + 2R_1R_2NH \leftrightarrow R_1R_2NCOO^- + R_1R_2NH_2^+ \quad \text{(R1.2)}$$

2. Bicarbonate formation with OH^-:

$$CO_2 + OH^- \leftrightarrow HCO_3^- \quad \text{(R1.3)}$$

3. Bicarbonate formation with H_2O:

$$CO_2 + H_2O + HCO_3^- + H^+ \quad \text{(R1.4)}$$

4. Alkylcarbonate formation:

$$CO_2 + R_1R_2C(-OH) - CH_2 - NH + OH^-$$

$$\leftrightarrow R_1R_2 - C(-O - CO_2^-) - CH_2 - NH + H_2O \quad \text{(R1.5)}$$

1.3 Amine concentration and CO_2 capture

To evaluate the effect of amine concentration on capturing carbon dioxide, it has been reported a study including AMP+PZ. During this measurement, the weight of total amine was kept at 30%, and 40%. Moreover, the ratio of L/G was constant at 3, and 2 (mol/mol). Figure 1.7 shows the percentage of CO_2 capture at 30 wt% aqueous amine with the L/G ratio at 3 [20].

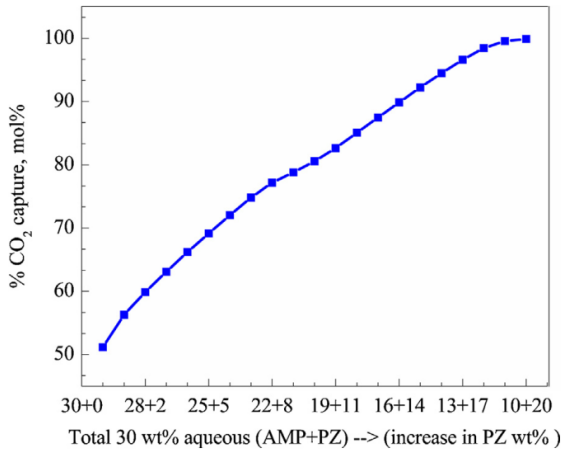

Figure 1.7: CO_2 capture rate with 30 wt% (AMP+PZ) and L/G=3 [20].

The result of %CO_2 capture at 40 wt% aqueous amine with the L/G ratio at 2 illustrates in Figure 1.8.

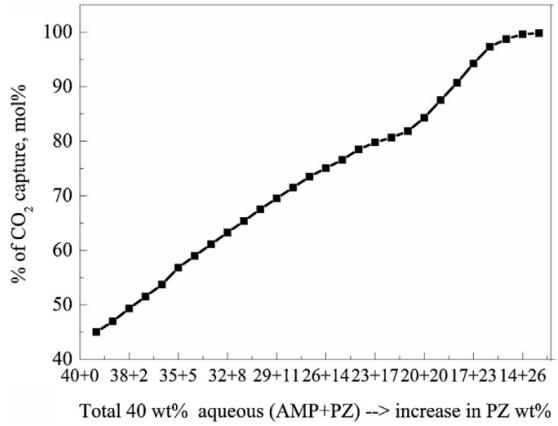

Figure 1.8: CO_2 capture rate with 40 wt% (AMP+PZ) and L/G=2 [20].

1.4 Corrosivity of amine solution in CO_2 capture

In the process of carbon dioxide capture, corrosion is a parameter due to the components of amine solutions. It has been reported that approximately 25% of the cost of maintenance dedicates to corrosion control. Many factors influence the rate of corrosivity such as the temperature of the process, type and concentration of the used amine, and amount of CO_2. The rate of corrosiveness is ranked, and Table 1.1 explains it in order of single and blended amines [21]. Some SEM images of corrosion are presented in Appendix A.

Table 1.1: Corrosivity of amine systems in CO_2 capture [21].

Amine type	Corrosivity order
Single amine	MEA > AMP > DEA > PZ > MDEA
Blended amines	MEA-PZ > MEA-AMP > MEA-MDEA > MDEA-PZ > AMP-PZ

1.5 CESAR1 solvent analysis

To evaluate CESAR1 solvent, several methods implement to examine the effects of CO_2 loaded into the solvent and how much the AMP+PZ solution can capture carbon dioxide. Regarding this aim, Fourier Transform Infrared Spectroscopy (FTIR), Nuclear Magnetic Resonance (NMR), and Multivariate data analysis (PLS-R) have been used.

1.5.1 Fourier Transform Infrared Spectroscopy (FTIR)

Fourier Transform Infrared Spectroscopy (FTIR) measures the infrared region of the electromagnetic radiation spectrum. FTIR is a straightforward method to determine the functional groups' composition and identify as well as quantify the compounds in a sample [9,22]. This method has a lower frequency and a longer wavelength than visible light. wavelength can be measured by passing infrared radiation through the sample. Therefore, the sample absorbs light at various frequencies based on the molecular structure. The functional groups in the sample are determined based on the wavelength of the reflected radiation [23].
FTIR device equipped with a detector MCT (mercury cadmium telluride) and resolution and spectra ranges is 4 cm^{-1} and 400-4000 cm^{-1}, respectively [24].

1.5.2 Multivariate data analysis

Multivariate data analysis namely unscrambler used for analyzing objects based on prediction and is useful to develop mathematical models. One of the common methods in multivariate calibration is PLS-R (Partial least squares regression). Cross-validation is commonly used in PLS to predict the calibration's average performance. The predictor matrix X and the response vector Y are described as linear combinations of orthogonal components in PLS regression [25]. Y is predicted by selecting a set of orthogonal elements known as latent variables from the predictors, X, and increasing the covariance between X and Y. All variables are maintained in PLS-R. The model includes related variables with relevant weights, while the model includes unrelated variables with irrelevant weights [26]. The analysis demonstrates four different plots including score, regression coefficients (R^2), RMSE (root mean square error), and predicted vs. reference.

2 Materials and methods

In this section, it is going to explain about all devices, methods and chemical materials had been used in the project

2.1 CESAR1

The object of the project was to compare CESAR1 solution in two different ways, including loaded with and without CO_2, and examine the effect of loaded CO_2 weight on several parameters such as pH, density, and ingredients of the samples by FTIR test.

2.1.1 Solution preparation

To prepare the CESAR1 solution, it used 270 gr of 2-amino-2-methyl-1-propanol (AMP), 130 gr of piperazine (PZ), and 600 gr of distilled water (H_2O). These amounts gave 1 kg of CESAR1 solution. Figure 2.1 shows three different beakers including the mentioned constituents.

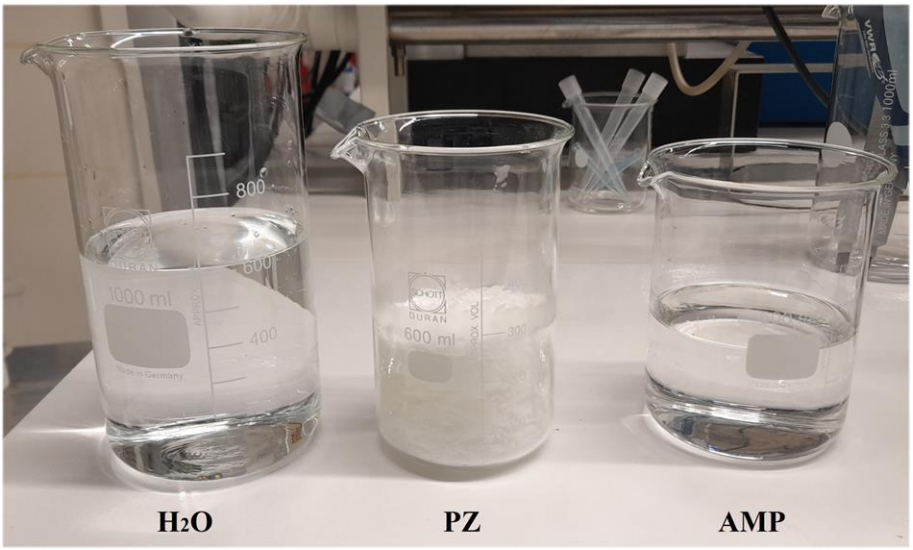

Figure 2.1: CESAR1 preparation constituents.

2.1.2 CO_2 loading

The prepared unloaded CESAR1 solution was loaded with carbon dioxide. It was planned to load 87 g of CO_2 for the 1 kg of the solution, but it had been added 87.68 g of CO_2 to the solution practically. Figure 2.2 presents the set-up used for CO_2 loading.

Figure 2.2: CO_2 loading instrument.

2.1.3 Fourier transform infrared spectroscopy (FTIR) samples

To analyze ingredients of loaded as well as unloaded CESAR1, 44 samples were prepared based on different solutions. As Figure 2.3 shows, each sample consists of 25 g CESAR1 with various loaded and unloaded solutions. In other words, it has been blended to evaluate the effect of CO_2 on the solution. The first sample of this series included 25 g of unloaded CESAR1. For the rest of the samples, it added 0.25 g approximately of loaded CESAR1 continuously until the last one with 25 g of loaded CESAR1.

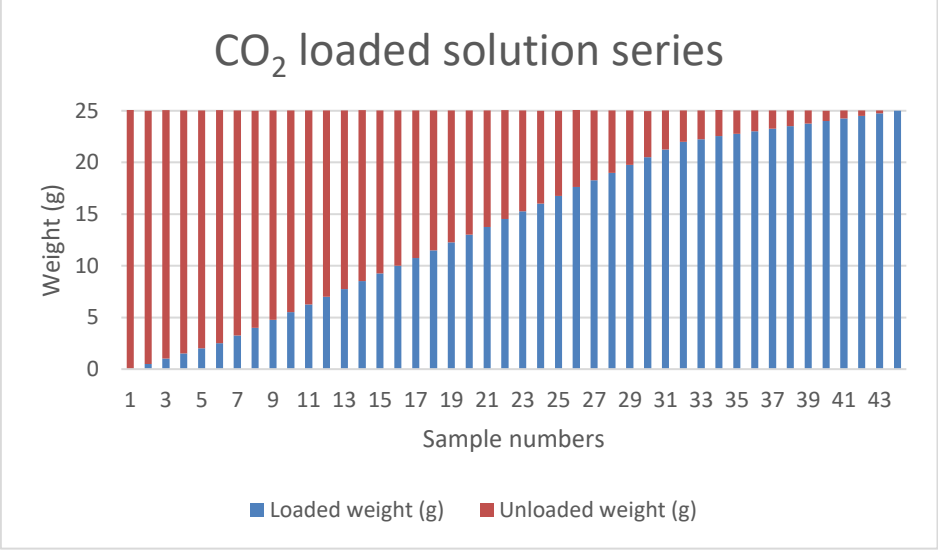

Figure 2.3: Sample series of CO_2 loading.

2.2 Fourier transform infrared spectroscopy (FTIR)

FTIR spectrometer model MB-3000 of ABB company was used for characterization. The device configuration includes calibration of an empty cell at scan step of 20 and wavelength span between 400 – 4000 cm^{-1}. This is used as a reference spectrum in the database.
All 44 samples were analyzed by FTIR and examined the influence of loaded solution amount into the sample on the plot. A drop of the sample was placed on the ATR crystal and covered by a metal lid. The experiment parameters are presented in Table 2.1.

Table 2.1: Experimental parameters of FTIR test.

No.	Parameter	Value
1	Resolution	8
2	Scans	20
3	Measurement interval	0.1 min
4	Acquisition mode	Absorbance
5	Wavelength range	400 – 4000 cm^{-1}
6	Detector first gain	671.41
7	Detector number	1

2.3 pH measurement

This test was performed for CESAR1 solutions with various CO_2 amounts to evaluate how much the CO_2 loaded could affect the pH value. It employed the pH probes of the same device for titration and measured all samples. Figure 2.4 illustrates the probes for measuring the pH of the solutions.

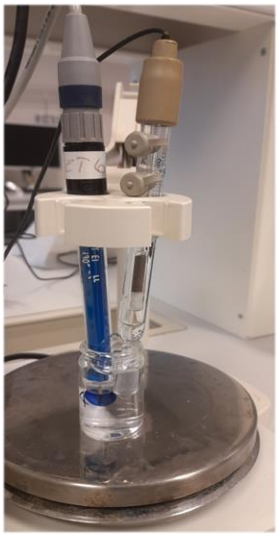

Figure 2.4: pH probes for pH measurement.

2.4 Partial Least-Squares Regression (PLS-R)

PLS-R model preparation was performed by Unscrambler X version 10.3. It is considered a test matrix for validation to avoid any optimistic results as well as to acquire a more realistic analysis. According to 44 available samples, it was defined two ranges for rows of data including calibration set (odd samples), and validation set (even samples). It selected two main sets for the elements that contributed to the analysis. Calibration sets were employed for odd samples, whereas the validation set used even samples. Each set contained 22 samples and the algorithm utilized was NIPALS (nonlinear iterative partial least squares algorithm). This is a common algorithm that uses for PLSR to compute components with orthogonal vectors.

Moreover, plotting results of FTIR in form of a line graph gave an overview of picks that showed the most important constituents. Afterward, it was separated all the picks on the line graph into another individual line plot regarding some literature reviews that defined the considerable wavenumbers of compositions.

Finally, the results of PLS-R are presented in 4 different axes based on the T-U plot, Loadings, RMSE (Root Mean Square Error), and Predicted versus Reference.

By removing outliers in T-U as well as Predicted versus Reference plots, checking the most valuable factors, correlation, and slope values, I could consequence the how extent did the analysis was accurate. Because a model based on existing outliers makes an unstable prediction with error.

2.5 Density measurement

To analyze the density of samples, it employed a device namely “Anton Paar” (Figure 2.5) which could be utilized for both low- and high-pressure situations. Based on the aim of the project, it used low-pressure measurement.

Before measuring the density, checking the calibration and density was necessary. The index sample to calibrate the device was distilled water. The calibration step started with washing the U-tube inside the device by injection.

Firstly, the tube was washed with distilled water and secondly, ethanol was injected to clean the water inside the U-tube. Finally, an air pump dried the tube for 15 minutes to get prepared it for injection of the sample. The process of washing the tube was implemented after measuring the density of each sample.

It was selective samples for this measurement (odd and the last samples) and it has been used interpolation method to reach the density values of even samples. The temperatures considered for this measurement were 20 and 40 °C and each sample had two different density values regarding the temperatures.

Figure 2.5: Density measurement device.

3 Results

3.1 FTIR

Table 3.1 illustrates the wavelengths and the species of CESAR1 aqueous solution including the numbers of picks during the FTIR test. Moreover, the wavelengths of this study were compared with many literature reviews to check the accuracy of this analysis.

Table 3.1: Vibrational test of CESAR1 and the species.

No. of picks	Wavelength [cm^{-1}]	Wavelength [cm^{-1}] (Literature review)	Species formula
1	995	985-995 [27]	C−H out-of-plane bend
2	1049	1043-1049 [9,28,29] 1043 [30]	C−N, C−O bending, hydroxyl, AMP
	1053	1052 [31] 1054 [9]	C−O AMPCOO− AMPH+
	1072	1072 [9]	C−N Carbamate AMPCOO− AMPH+
	1076	1076 [30]	C−N
	1095	1095 [32]	C-C stretching
3	1126	1116 [33] 1119 [32] 1159 [33]	C−O stretching
	1130		
	1134		

4	1234	1235-1245 [34]	C−N stretching
5	1261	1260 [28,29,35,36]	C−O bending
		1265 [9]	$N - COO^-$ PZCOO−
6	1319	1315-1330 [34]	C−O vibration
	1323		
	1327	1327 [37]	
7	1377	1370 [38]	C−O stretching
	1384	1382 [30]	Carbonate HCO_3^-
	1388	1388 [39]	C−H stretching
8	1415	1410 [40,41]	C=O symmetric stretching
9	1469	1460 [42] 1461 [32] 1464 [33]	C−H banding
		1470 [9]	NH_2^+ PZH+ +HPZH+
10	1508	1500 [37]	C=C aromatic
	1523	1524 [9]	COO− Carbamate
			PZCOO−

			Monocarbamate
	1535	1535 [43]	C−N stretching
	1550	1546 [9]	COO− Carbamate
		1548-1550 [31]	−OOCPZCOO− Di-carbamate N−H C−N
	1558	1555 [40]	C=O asymmetric stretching
11	1635	1635 [44]	Water
		1620-1640 [37,42] 1620 [37]	O-H bending Hydroxyl or water,
		1628 [9]	H-O-H
	1643	1645 [30]	$N-H$
	1647		
	1651	1650 [45,46]	C=O stretching of amide
	1658	1657 [32] 1655 [33] 1654 [32]	C=C stretching

3.2 pH measurement

Measured values of the pH for 44 different CESAR1 samples are illustrated in Figure 3.1. As shown, the highest value of pH belongs to sample 1 (25 g of unloaded CESAR1) with 12.6. The more added loaded solution to the sample, the less the pH value is in the line graph. It can be deducted that 25 grams of unloaded as well as loaded samples with CO_2 (samples 1 and 44) have about 3 values difference in their pH from 12.6 to 9.7 respectively.

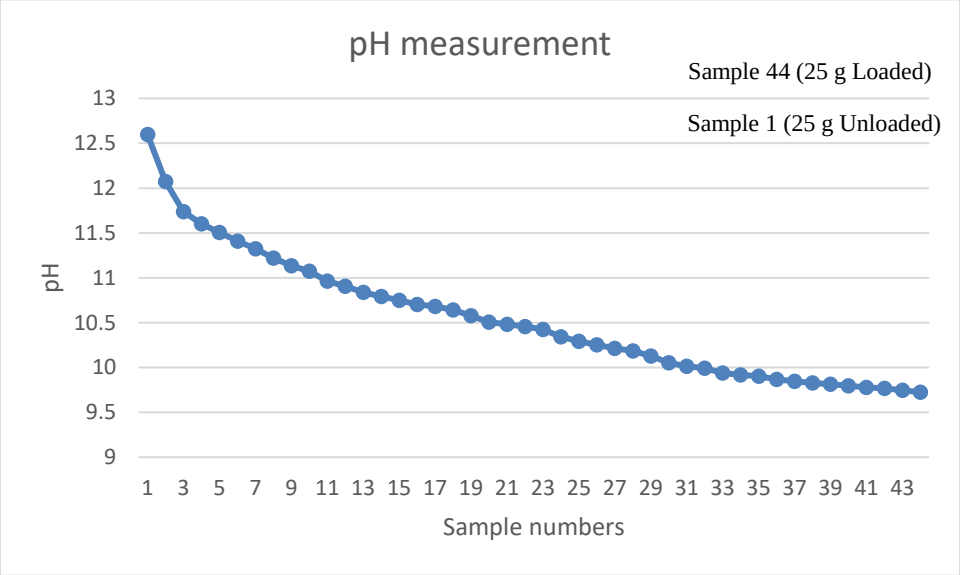

Figure 3.1: pH measurement results.

3.3 FTIR analysis

The compositions of the samples have been determined by the FTIR method and the following figures illustrate several characterizations of CESAR1 solvent. The considerable region in this project is between 950 to 1700 cm^{-1} and all the remarkable picks are identified in the mentioned wavelengths. Figure 3.2 illustrates the whole noticeable areas of the study and there are some main picks that are marked with their wavelengths to discriminate the unloaded as well as loaded samples.

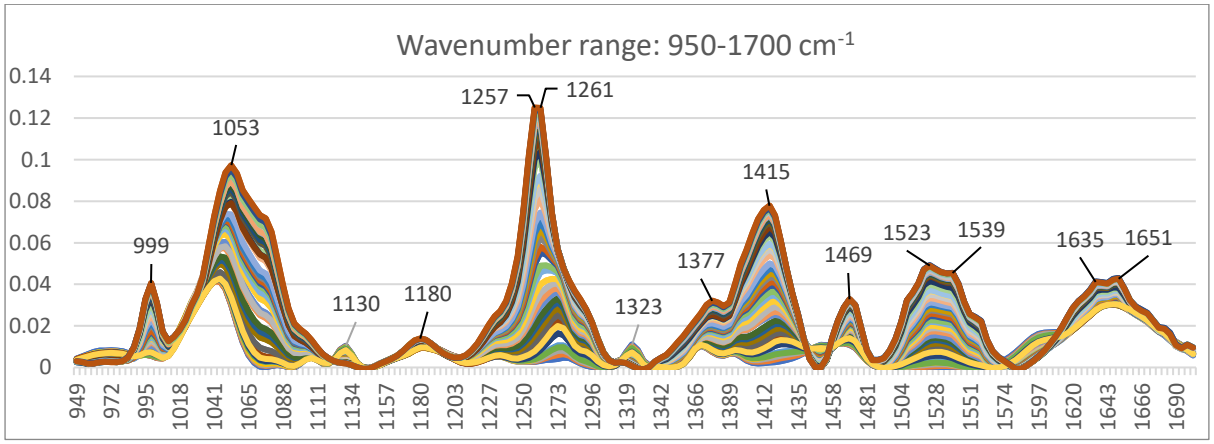

Figure 3.2: The wavelength range of FTIR analysis for CESAR1 solvent.

Figure 3.3 can show clearly that the highest loaded sample (number 44) generated the highest picks in the plot, while sample number 1 did not affect picks dramatically. In other words, the more added CO_2-loaded solvent, the higher pick generates in the FTIR plot.

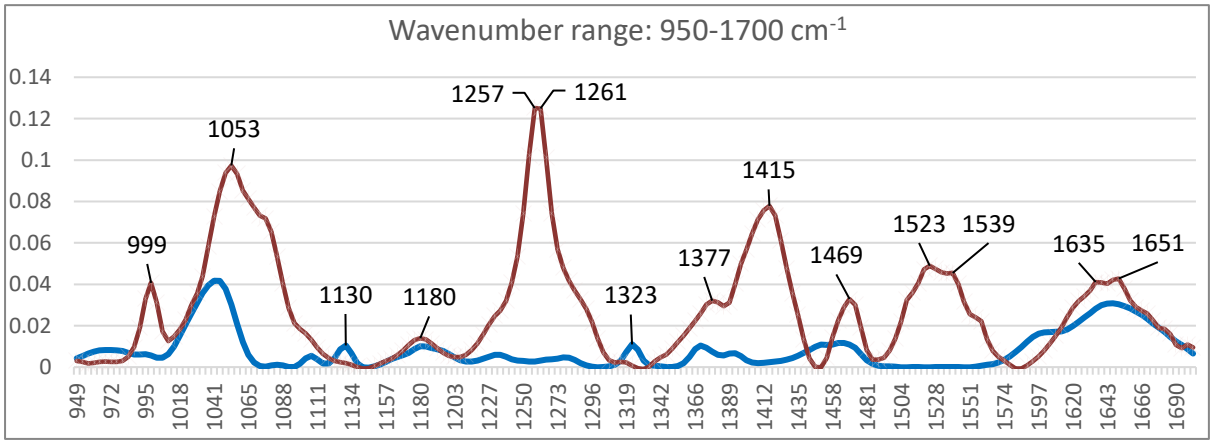

Figure 3.3: The two highest and lowest picks regarding the unloaded and loaded samples.

According to literature reviews, each pick corresponds to some earmarked compositions, and it is recognized in 7 significant picks. The wavelength regions and the bonds are shown in Figure 3.4.

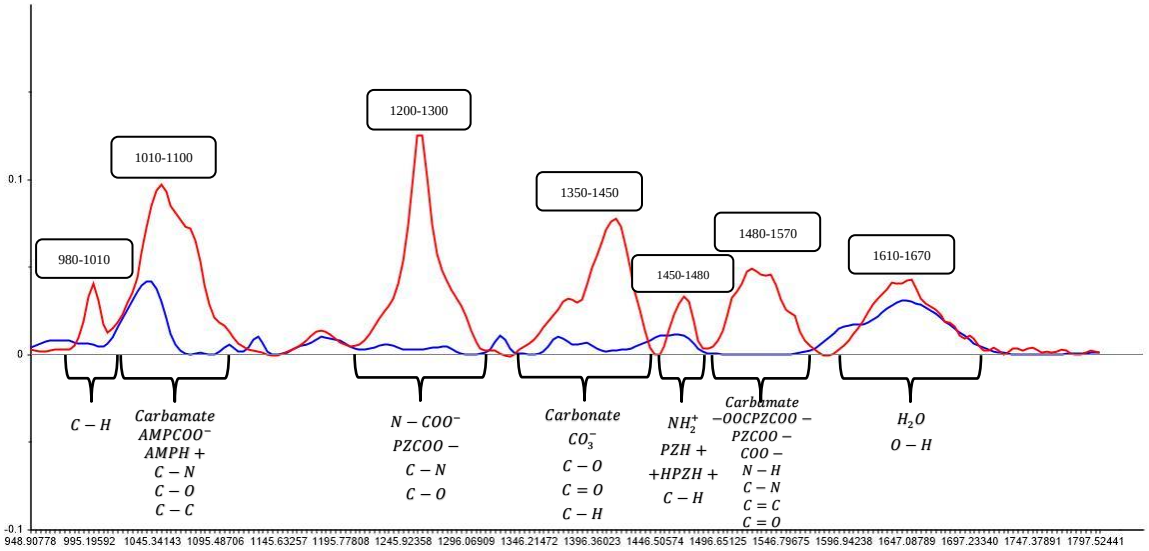

Figure 3.4: Corresponding wavelengths to the constituents of solvent.

3.4 PLS-R analysis based on the FTIR outlet

The results of the unscrambler analysis are represented based on several objectives as the Figures below clarify.

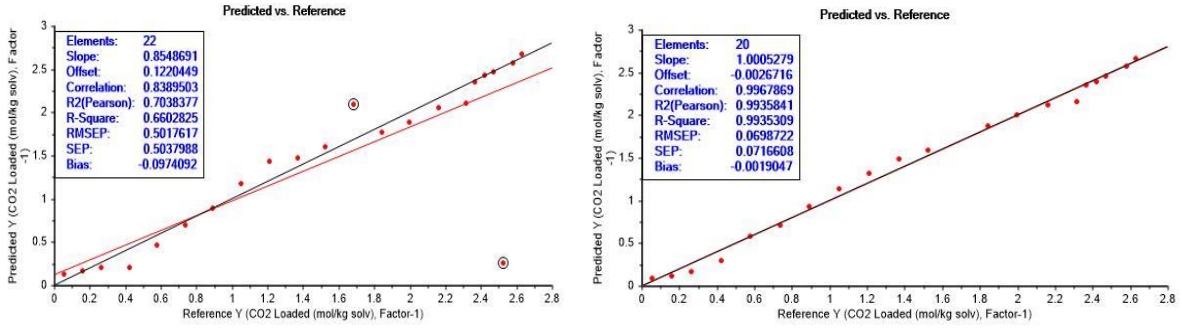

(a) (b)

Figure 3.5: Predicted vs. Reference plot with outliers (Wavelength range: 400-4000 cm^{-1}) [mol/kg solvent]; (a) and without outliers (Wavelength range: 950-1600 cm^{-1}) [mol/kg solvent]; (b).

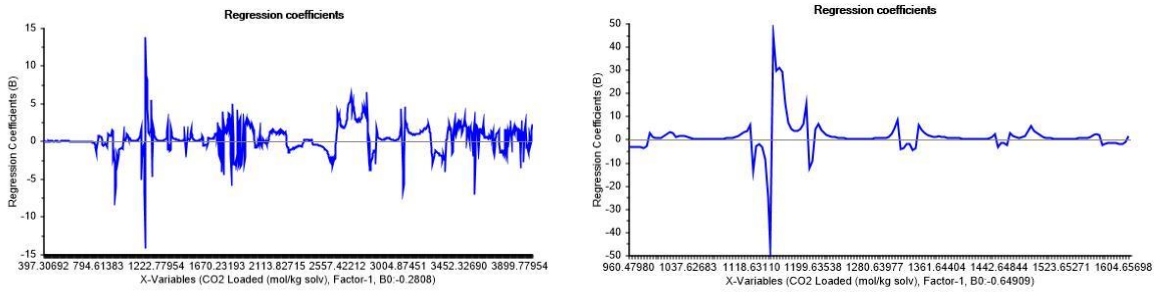

(a) (b)

Figure 3.6: Regression coefficients plots with outliers (Wavelength range: 400-4000 cm^{-1}) [mol/kg solvent]; (a) and without outliers (Wavelength range: 950-1600 cm^{-1}) [mol/kg solvent]; (b).

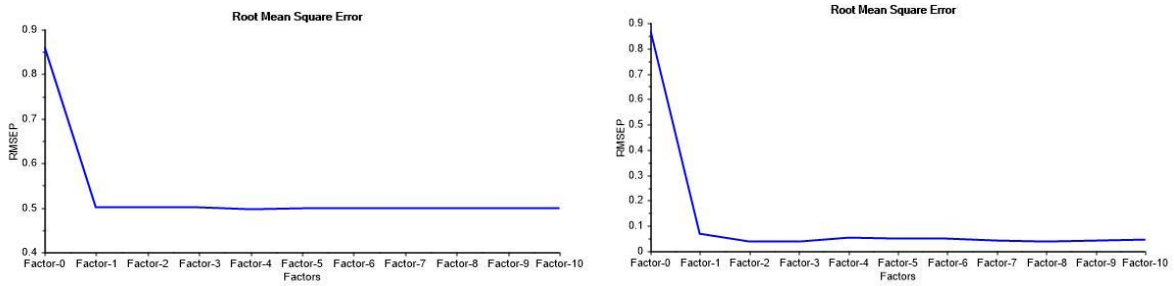

(a) (b)

Figure 3.7: RMSE plots with outliers (Wavelength range: 400-4000 cm^{-1}) [mol/kg solvent]; (a) and without outliers (Wavelength range: 950-1600 cm^{-1}) [mol/kg solvent]; (b).

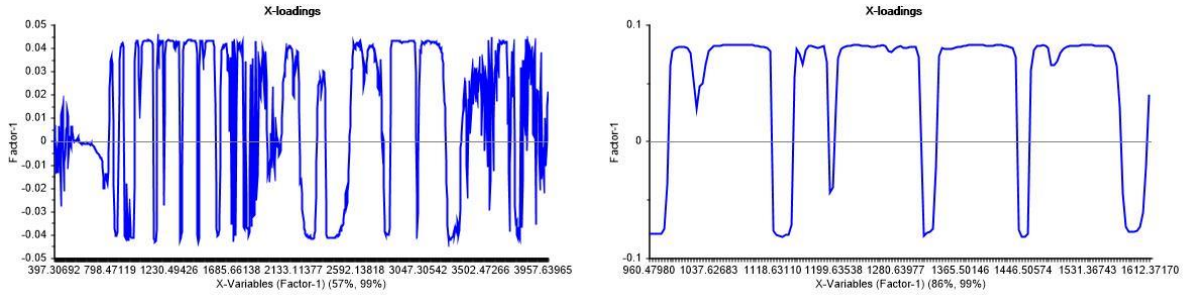

(a) (b)

Figure 3.8: X-loading plots with outliers (Wavelength range: 400-4000 cm^{-1}) [mol/kg solvent]; (a) and without outliers (Wavelength range: 950-1600 cm^{-1}) [mol/kg solvent]; (b).

3.5 Density measurement

The density values of samples are presented in Figure 3.9. It illustrates that sample 1 with unloaded solution (25 g without CO_2) has the least value of density (0.99 and 1.01 g/cm^3 at 40 and 20 °C respectively), whereas the sample 44 with 25 g of fully CO_2 loaded CESAR1 is 1.10 as well as 1.09 g/cm^3 for the temperatures 20 and 40 °C. In the case of the temperature, the difference between the measured densities for each sample is approximately 0.01 g/cm^3. It means these two lines of density measurements had roughly 0.01 g/cm^3 in the entire investigation. The density was always lower at 40 in comparison to 20 °C.

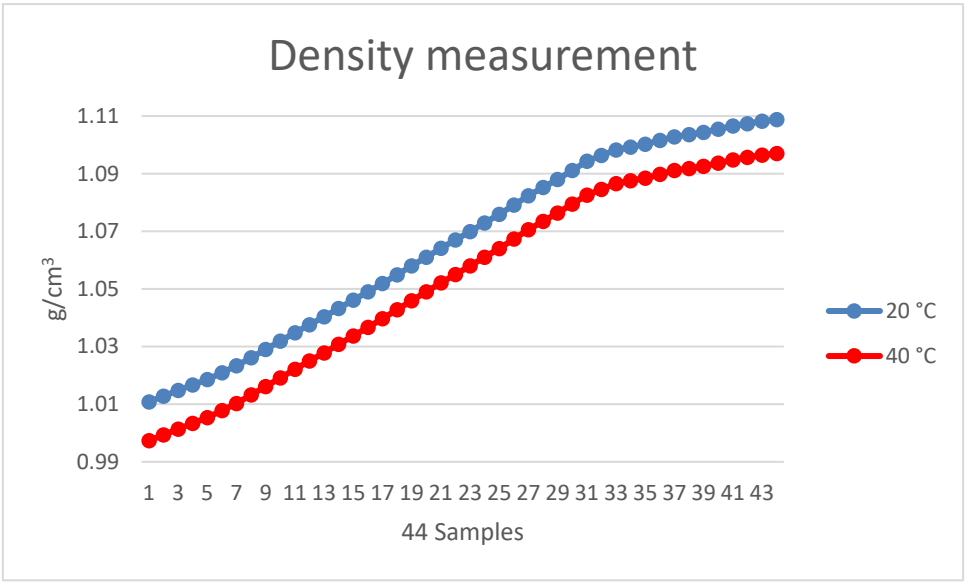

Figure 3.9: Density measurements of loading CO_2 in CESAR1 in two different temperatures.

4 Discussion

Evaluating the CESAR1 solution indicates that it can be considered as a high potential aqueous carbon dioxide capture. CO_2 absorption is significantly affected by applying the blend of AMP and PZ as the CESAR1.
Loading carbon dioxide was run in different ranges of weights to reach the effect of loaded CO_2 on the parameters pH as well as density. Figure 3.1 shows that pH measurements for CESAR1 follow the rule that the more CO_2 loaded, the less pH value. However, Figure 3.9 proves that CO_2 loading shows the reverse result for density measurement. The findings show that the density study for the fully loaded CESAR1 with carbon dioxide has the highest value for density measurement in comparison to the pH test.

Peaks in the FTIR analysis show that CESAR1 is actively reacting to the applied loaded CO_2. According to Figure 3.2, several different wavelength ranges were picked for the chemical decomposition of CESAR1. Findings from the FTIR study give an idea about the last pick that it is related to water which is not notable and was removed from the test.

FTIR spectra of CESAR1 samples showed some stretching groups including C-N, C-H, C-C, C-O, C=O, C=C, and N-H. As Table 3.1 demonstrates, carbonate, carbamate, monocarbamate, and di-carbamate were recognized during FTIR analysis. Therefore, this method is promising because of its simplicity, efficiency, and the mild reaction conditions needed. Chemical characterization by FTIR is found to be a simple, cheap, and fast method to identify the functional groups in this aqueous solution. An attempt to quantify the functional groups in CESAR1 with the FTIR results has been tried. Indeed, looking at the FTIR graph (Figure 3.4) gives several picks of the intensity of each functional group.
Results from PLS-R represented in Figures 3.5, 3.6, 3.7, and 3.8, illustrate wavelength ranges between 400 and 4000 cm^{-1} with outliers and 950 and 1600 cm^{-1} without outliers.
Since many picks can share the same functional groups, quantification of functional groups is not enough to fully characterize the specific chemical components in the CESAR1 solution. Because of this limitation, NMR could report more information about the concentration of each component, however, the NMR results did not prepare and this study has not been done as it requires more specialized knowledge in this area.

5 Conclusion

CESAR1 could be a promising solution due to its renewability, environmentally friendly nature, and compatibility with existing technologies to capture carbon dioxide.
Among the carbon capture techniques, CESAR1 (AMP+PZ) mitigates high energy requirements and causes to react CO_2 with PZ more with high CO_2 loading capacity. It is proved that PZ has a considerable effect on the rate of CO_2 capture and can enhance it even if is a small amount. pH and density measurements were selected to evaluate the CESAR1 solution. The best results were observed for sample 44 because of its highest loaded CO_2 during the FTIR tests. Findings illustrate that if the CO_2-loaded solution adds to the sample, it will give the highest pick in the FTIR curve.
The effect of the different methods on the AMP+PZ (CESAR1) is evaluated by applying pH analysis. The results determine the effect of the CO_2 loading on the solution is considerably different from the density evaluation. The test clarified the most loaded carbon dioxide, the least value in pH measurement. However, the highest components of CO_2 increased the density amount of the solution. Thus, a thorough study of each method is recommended, especially for density as well as pH measurements.

According to Figure 3.5 for PLS-R analysis, the results obtained for 22 elements were considerably had less correlation (83%). By removing the outliers and decreasing the elements to 20, it has caused a more accurate correlation of approximately 99%. As a consequence, lower numbers of outliers, eventuate in more effective as well as a realistic predictions.

Consequently, the FTIR and PLS-R may have clarified the characteristics of the CESAR1. Better results could be obtained with NMR and the concentration of each component in the solution.

References

(1) Shakerian, F.; Kim, K.-H.; Szulejko, J. E.; Park, J.-W. A Comparative Review between Amines and Ammonia as Sorptive Media for Post-Combustion CO2 Capture. *Applied Energy* **2015**, *148*, 10–22. https://doi.org/10.1016/j.apenergy.2015.03.026.

(2) Nwaoha, C.; Supap, T.; Idem, R.; Saiwan, C.; Tontiwachwuthikul, P.; AL-Marri, M. J.; Benamor, A. Advancement and New Perspectives of Using Formulated Reactive Amine Blends for Post-Combustion Carbon Dioxide (CO2) Capture Technologies. *Petroleum* **2017**, *3* (1), 10–36. https://doi.org/10.1016/j.petlm.2016.11.002.

(3) Kanniche, M.; Gros-Bonnivard, R.; Jaud, P.; Valle-Marcos, J.; Amann, J.-M.; Bouallou, C. Pre-Combustion, Post-Combustion and Oxy-Combustion in Thermal Power Plant for CO2 Capture. *Applied Thermal Engineering* **2010**, *30* (1), 53–62. https://doi.org/10.1016/j.applthermaleng.2009.05.005.

(4) Wong, M. K.; Bustam, M. A.; Shariff, A. M. Chemical Speciation of CO2 Absorption in Aqueous Monoethanolamine Investigated by in Situ Raman Spectroscopy. *International Journal of Greenhouse Gas Control* **2015**, *39*, 139–147. https://doi.org/10.1016/j.ijggc.2015.05.016.

(5) Dash, S. K.; Samanta, A. N.; Bandyopadhyay, S. S. (Vapour+liquid) Equilibria (VLE) of CO2 in Aqueous Solutions of 2-Amino-2-Methyl-1-Propanol: New Data and Modelling Using ENRTL-Equation. *The Journal of Chemical Thermodynamics* **2011**, *43* (8), 1278–1285. https://doi.org/10.1016/j.jct.2011.03.016.

(6) Sun, W.-C.; Yong, C.-B.; Li, M.-H. Kinetics of the Absorption of Carbon Dioxide into Mixed Aqueous Solutions of 2-Amino-2-Methyl-l-Propanol and Piperazine. *Chemical Engineering Science* **2005**, *60* (2), 503–516. https://doi.org/10.1016/j.ces.2004.08.012.

(7) Li, H.; Moullec, Y. L.; Lu, J.; Chen, J.; Marcos, J. C. V.; Chen, G. Solubility and Energy Analysis for CO2 Absorption in Piperazine Derivatives and Their Mixtures. *International Journal of Greenhouse Gas Control* **2014**, *31*, 25–32. https://doi.org/10.1016/j.ijggc.2014.09.012.

(8) Brúder, P.; Grimstvedt, A.; Mejdell, T.; Svendsen, H. F. CO2 Capture into Aqueous Solutions of Piperazine Activated 2-Amino-2-Methyl-1-Propanol. *Chemical Engineering Science* **2011**, *66* (23), 6193–6198. https://doi.org/10.1016/j.ces.2011.08.051.

(9) Zanone, A.; Tavares, D. T.; Paiva, J. L. de. An FTIR Spectroscopic Study and Quantification of 2-Amino-2-Methyl-1-Propanol, Piperazine and Absorbed Carbon Dioxide in Concentrated Aqueous Solutions. *Vibrational Spectroscopy* **2018**, *99*, 156–161. https://doi.org/10.1016/j.vibspec.2018.03.007.

(10) Akanksha; Pant, K. K.; Srivastava, V. K. Carbon Dioxide Absorption into Monoethanolamine in a Continuous Film Contactor. *Chemical Engineering Journal* **2007**, *133* (1), 229–237. https://doi.org/10.1016/j.cej.2007.02.001.

(11) Moser, P.; Wiechers, G.; Schmidt, S.; Monteiro, J. G. M.-S.; Goetheer, E.; Charalambous, C.; Saleh, A.; van der Spek, M.; Garcia, S. ALIGN-CCUS: Results of the 18-Month Test with Aqueous AMP/PZ Solvent at the Pilot Plant at Niederaussem –

Solvent Management, Emissions and Dynamic Behavior. *International Journal of Greenhouse Gas Control* **2021**, *109*, 103381. https://doi.org/10.1016/j.ijggc.2021.103381.

(12) Sartori, G.; Savage, D. W. Sterically Hindered Amines for Carbon Dioxide Removal from Gases. *Ind. Eng. Chem. Fund.* **1983**, *22* (2), 239–249. https://doi.org/10.1021/i100010a016.

(13) Li, H.; Frailie, P. T.; Rochelle, G. T.; Chen, J. Thermodynamic Modeling of Piperazine/2-Aminomethylpropanol/CO2/Water. *Chemical Engineering Science* **2014**, *117*, 331–341. https://doi.org/10.1016/j.ces.2014.06.026.

(14) Freeman, S. A.; Dugas, R.; Van Wagener, D.; Nguyen, T.; Rochelle, G. T. Carbon Dioxide Capture with Concentrated, Aqueous Piperazine. *Energy Procedia* **2009**, *1* (1), 1489–1496. https://doi.org/10.1016/j.egypro.2009.01.195.

(15) Mangalapally, H. P.; Hasse, H. Pilot Plant Study of Two New Solvents for Post Combustion Carbon Dioxide Capture by Reactive Absorption and Comparison to Monoethanolamine. *Chemical Engineering Science* **2011**, *66* (22), 5512–5522. https://doi.org/10.1016/j.ces.2011.06.054.

(16) Aroonwilas, A.; Tontiwachwuthikul, P. High-Efficiency Structured Packing for CO2 Separation Using 2-Amino-2-Methyl-1-Propanol (AMP). *Separation and Purification Technology* **1997**, *12* (1), 67–79. https://doi.org/10.1016/S1383-5866(97)00037-3.

(17) Artanto, Y.; Jansen, J.; Pearson, P.; Puxty, G.; Cottrell, A.; Meuleman, E.; Feron, P. Pilot-Scale Evaluation of AMP/PZ to Capture CO2 from Flue Gas of an Australian Brown Coal–Fired Power Station. *International Journal of Greenhouse Gas Control* **2014**, *20*, 189–195. https://doi.org/10.1016/j.ijggc.2013.11.002.

(18) Dey, A.; Aroonwilas, A. CO2 Absorption into MEA-AMP Blend: Mass Transfer and Absorber Height Index. *Energy Procedia* **2009**, *1* (1), 211–215. https://doi.org/10.1016/j.egypro.2009.01.030.

(19) Godini, H. R.; Mowla, D. Selectivity Study of H2S and CO2 Absorption from Gaseous Mixtures by MEA in Packed Beds. *Chemical Engineering Research and Design* **2008**, *86* (4), 401–409. https://doi.org/10.1016/j.cherd.2007.11.012.

(20) Dash, S. K.; Samanta, A. N.; Bandyopadhyay, S. S. Simulation and Parametric Study of Post Combustion CO2 Capture Process Using (AMP+PZ) Blended Solvent. *International Journal of Greenhouse Gas Control* **2014**, *21*, 130–139. https://doi.org/10.1016/j.ijggc.2013.12.003.

(21) Gunasekaran, P.; Veawab, A.; Aroonwilas, A. Corrosivity of Single and Blended Amines in CO2 Capture Process. *Energy Procedia* **2013**, *37*, 2094–2099. https://doi.org/10.1016/j.egypro.2013.06.088.

(22) Lievens, C.; Mourant, D.; He, M.; Gunawan, R.; Li, X.; Li, C.-Z. An FT-IR Spectroscopic Study of Carbonyl Functionalities in Bio-Oils. *Fuel* **2011**, *90* (11), 3417–3423. https://doi.org/10.1016/j.fuel.2011.06.001.

(23) Xu, F.; Xu, Y.; Lu, R.; Sheng, G.-P.; Yu, H.-Q. Elucidation of the Thermal Deterioration Mechanism of Bio-Oil Pyrolyzed from Rice Husk Using Fourier Transform Infrared Spectroscopy. *J. Agric. Food Chem.* **2011**, *59* (17), 9243–9249. https://doi.org/10.1021/jf202198u.

(24) Kumar, P. K.; Vijaya Krishna, S.; Verma, K.; Pooja, K.; Bhagawan, D.; Himabindu, V. Phycoremediation of Sewage Wastewater and Industrial Flue Gases for Biomass Generation from Microalgae. *South African Journal of Chemical Engineering* **2018**, *25*, 133–146. https://doi.org/10.1016/j.sajce.2018.04.006.

(25) De Vries, S.; J.F. Ter Braak, C. Prediction Error in Partial Least Squares Regression: A Critique on the Deviation Used in The Unscrambler. *Chemometrics and Intelligent Laboratory Systems* **1995**, *30* (2), 239–245. https://doi.org/10.1016/0169-7439(95)00030-5.

(26) Aïchi, H.; Fouad, Y.; Causeur, D.; Walter, C. Organic Carbon and Total Iron Effect on Soil Vis-SWNIR Spectraand Quantification of Their Contents Using PLS R Models. *Communications in Soil Science and Plant Analysis* **2020**, *51* (9), 1253–1267. https://doi.org/10.1080/00103624.2020.1751187.

(27) Coates, J.; Meyers (ed, R. A.; Wiley, J.; Coates, J. Molecular Backbone 6.

(28) Shenderova, O.; Panich, A. M.; Moseenkov, S.; Hens, S. C.; Kuznetsov, V.; Vieth, H.-M. Hydroxylated Detonation Nanodiamond: FTIR, XPS, and NMR Studies. *J. Phys. Chem. C* **2011**, *115* (39), 19005–19011. https://doi.org/10.1021/jp205389m.

(29) Jiang, T.; Xu, K. FTIR Study of Ultradispersed Diamond Powder Synthesized by Explosive Detonation. *Carbon* **1995**, *33* (12), 1663–1671. https://doi.org/10.1016/0008-6223(95)00115-1.

(30) Richner, G.; Puxty, G. Assessing the Chemical Speciation during CO2 Absorption by Aqueous Amines Using in Situ FTIR. *Ind. Eng. Chem. Res.* **2012**, *51* (44), 14317–14324. https://doi.org/10.1021/ie302056f.

(31) Schmitt, J.; Flemming, H.-C. FTIR-Spectroscopy in Microbial and Material Analysis. *International Biodeterioration & Biodegradation* **1998**, *41* (1), 1–11. https://doi.org/10.1016/S0964-8305(98)80002-4.

(32) Valasi, L.; Kokotou, M. G.; Pappas, C. S. GC-MS, FTIR and Raman Spectroscopic Analysis of Fatty Acids of Pistacia Vera (Greek Variety “Aegina”) Oils from Two Consecutive Harvest Periods and Chemometric Differentiation of Oils Quality. *Food Research International* **2021**, *148*, 110590. https://doi.org/10.1016/j.foodres.2021.110590.

(33) Lim, S. Y.; Abdul Mutalib, M. S.; Khaza’ai, H.; Chang, S. K. Detection of Fresh Palm Oil Adulteration with Recycled Cooking Oil Using Fatty Acid Composition and FTIR Spectral Analysis. *International Journal of Food Properties* **2018**, *21* (1), 2428–2451. https://doi.org/10.1080/10942912.2018.1522332.

(34) Lin, Y.; Su, D. Fabrication of Nitrogen-Modified Annealed Nanodiamond with Improved Catalytic Activity. *ACS Nano* **2014**, *8* (8), 7823–7833. https://doi.org/10.1021/nn501286v.

(35) Martín, R.; Heydorn, P. C.; Alvaro, M.; Garcia, H. General Strategy for High-Density Covalent Functionalization of Diamond Nanoparticles Using Fenton Chemistry. *Chem. Mater.* **2009**, *21* (19), 4505–4514. https://doi.org/10.1021/cm9012602.

(36) Mitev, D.; Dimitrova, R.; Spassova, M.; Minchev, Ch.; Stavrev, S. Surface Peculiarities of Detonation Nanodiamonds in Dependence of Fabrication and Purification Methods.

Diamond and Related Materials **2007**, *16* (4), 776–780. https://doi.org/10.1016/j.diamond.2007.01.005.

(37) Lazzari, E.; Schena, T.; Marcelo, M. C. A.; Primaz, C. T.; Silva, A. N.; Ferrão, M. F.; Bjerk, T.; Caramão, E. B. Classification of Biomass through Their Pyrolytic Bio-Oil Composition Using FTIR and PCA Analysis. *Industrial Crops and Products* **2018**, *111*, 856–864. https://doi.org/10.1016/j.indcrop.2017.11.005.

(38) Wolcott, A.; Schiros, T.; Trusheim, M. E.; Chen, E. H.; Nordlund, D.; Diaz, R. E.; Gaathon, O.; Englund, D.; Owen, J. S. Surface Structure of Aerobically Oxidized Diamond Nanocrystals. *J. Phys. Chem. C* **2014**, *118* (46), 26695–26702. https://doi.org/10.1021/jp506992c.

(39) Suwanboon, S.; Amornpitoksuk, P.; Sukolrat, A.; Muensit, N. Optical and Photocatalytic Properties of La-Doped ZnO Nanoparticles Prepared via Precipitation and Mechanical Milling Method. *Ceramics International* **2013**, *39* (3), 2811–2819. https://doi.org/10.1016/j.ceramint.2012.09.050.

(40) Tu, J.-S.; Perevedentseva, E.; Chung, P.-H.; Cheng, C.-L. Size-Dependent Surface CO Stretching Frequency Investigations on Nanodiamond Particles. *J. Chem. Phys.* **2006**, *125* (17), 174713. https://doi.org/10.1063/1.2370880.

(41) Korobov, M. V.; Volkov, D. S.; Avramenko, N. V.; Belyaeva, L. A.; Semenyuk, P. I.; Proskurnin, M. A. Improving the Dispersity of Detonation Nanodiamond: Differential Scanning Calorimetry as a New Method of Controlling the Aggregation State of Nanodiamond Powders. *Nanoscale* **2013**, *5* (4), 1529–1536. https://doi.org/10.1039/C2NR33512C.

(42) Petit, T.; Puskar, L. FTIR Spectroscopy of Nanodiamonds: Methods and Interpretation. *Diamond and Related Materials* **2018**, *89*, 52–66. https://doi.org/10.1016/j.diamond.2018.08.005.

(43) Zhang, Q.; Mochalin, V. N.; Neitzel, I.; Knoke, I. Y.; Han, J.; Klug, C. A.; Zhou, J. G.; Lelkes, P. I.; Gogotsi, Y. Fluorescent PLLA-Nanodiamond Composites for Bone Tissue Engineering. *Biomaterials* **2011**, *32* (1), 87–94. https://doi.org/10.1016/j.biomaterials.2010.08.090.

(44) Srivastava, V.; Gusain, D.; Sharma, Y. C. Synthesis, Characterization and Application of Zinc Oxide Nanoparticles (n-ZnO). *Ceramics International* **2013**, *39* (8), 9803–9808. https://doi.org/10.1016/j.ceramint.2013.04.110.

(45) Jiang, T.; Xu, K.; Ji, S. FTIR Studies on the Spectral Changes of the Surface Functional Groups of Ultradispersed Diamond Powder Synthesized by Explosive Detonation after Treatment in Hydrogen, Nitrogen, Methane and Air at Different Temperatures. *J. Chem. Soc., Faraday Trans.* **1996**, *92* (18), 3401–3406. https://doi.org/10.1039/FT9969203401.

(46) Mochalin, V. N.; Neitzel, I.; Etzold, B. J. M.; Peterson, A.; Palmese, G.; Gogotsi, Y. Covalent Incorporation of Aminated Nanodiamond into an Epoxy Polymer Network. *ACS Nano* **2011**, *5* (9), 7494–7502. https://doi.org/10.1021/nn2024539.

Appendices

Appendix A: Corrosion images by SEM [21]

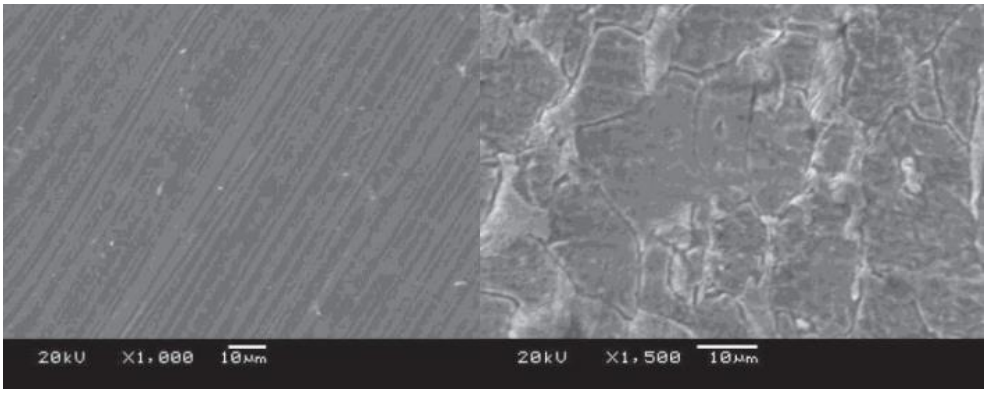

(a) (b)

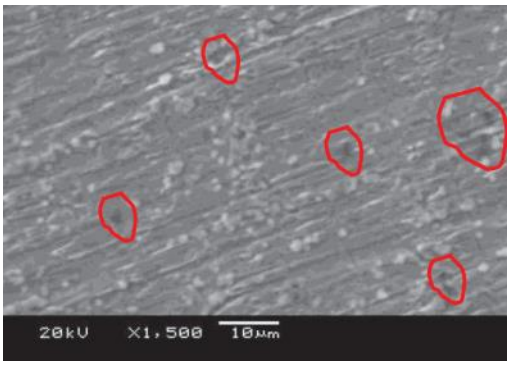

(c)

Figure A.1: (a) Fresh surface before the test; (b) corroded surface in DEA system; (c) corroded surface in PZ system. [21].